Supernova 2013by: A Type IIL Supernova with a IIP-like light curve drop[*]

S. Valenti[1,2][†], D. Sand[3], M. Stritzinger[4], D. A. Howell[1,2], I. Arcavi[1,5], C. McCully[1,2], M. J. Childress[6,7], E.Y. Hsiao[4,8], C. Contreras[4,8], N. Morrell[8], M. M. Phillips[8], M. Gromadzki[9,10], R. P. Kirshner[11], G. H. Marion[11,12]

[1] *Las Cumbres Observatory Global Telescope Network, 6740 Cortona Dr., Suite 102, Goleta, CA 93117, USA*
[2] *Department of Physics, University of California, Santa Barbara, Broida Hall, Mail Code 9530, Santa Barbara, CA 93106-9530, USA*
[3] *Physics Department, Texas Tech University, Lubbock, TX , 79409, USA*
[4] *Department of Physics and Astronomy, Aarhus University, Ny Munkegade 120, DK-8000 Aarhus C, Denmark*
[5] *Kavli Institute for Theoretical Physics, University of California, Santa Barbara, CA 93106, USA*
[6] *Research School of Astronomy and Astrophysics, Australian National University, Canberra, ACT 2611, Australia*
[7] *ARC Centre of Excellence for All-sky Astrophysics (CAASTRO); Australian National University; Canberra, ACT 2611, Australia*
[8] *Carnegie Observatories, Las Campanas Observatory, Colina El Pino, Casilla 601, Chile*
[9] *Millennium Institute of Astrophysics, Sotero Sanz 100, Oficina 104, Providencia, Santiago*
[10] *Instituto de Física y Astronomía, Universidad de Valparaíso, Av. Gran Bretaña 1111, Playa Ancha, Casilla, 5030, Chile*
[11] *Harvard-Smithsonian Center for Astrophysics, 60 Garden Street, Cambridge, MA 02138, USA)*
[12] *University of Texas at Austin, 1 University Station C1400, Austin, TX, 78712-0259, USA*

ABSTRACT

We present multi-band ultraviolet and optical light curves, as well as visual-wavelength and near-infrared spectroscopy of the Type II linear (IIL) supernova (SN) 2013by. We show that SN 2013by and other SNe IIL in the literature, after their linear decline phase that start after maximum, have a sharp light curve decline similar to that seen in Type II plateau (IIP) supernovae. This light curve feature has rarely been observed in other SNe IIL due to their relative rarity and the intrinsic faintness of this particular phase of the light curve. We suggest that the presence of this drop could be used as a physical parameter to distinguish between subclasses of SNe II, rather than their light curve decline rate shortly after peak. Close inspection of the spectra of SN 2013by indicate asymmetric line profiles and signatures of high-velocity hydrogen. Late ($\sim$ 90 days after explosion) near-infrared spectra of SN 2013by exhibit oxygen lines, indicating significant mixing within the ejecta. From the late-time light curve, we estimate that 0.029 $M_\odot$ of ^{56}Ni was synthesized during the explosion. It is also shown that the V-band light curve slope is responsible for part of the scatter in the luminosity (V magnitude 50 days after explosion) vs. ^{56}Ni relation. Our observations of SN 2013by and other SNe IIL through the onset of the nebular phase indicate that their progenitors are similar to those of SNe IIP.

Key words: supernovae: general – supernovae: SN 2013by, – galaxies:

1 INTRODUCTION

Type II supernovae (SNe II) have historically been divided into the Type IIL (linear) and Type IIP (plateau) subclasses based on the shape of their light curves in the weeks following explosion[1] (Barbon, Ciatti & Rosino 1979). SNe IIP light curves have

---

[*] This paper is based on observations gathered with: the LCOGT network of telescopes, the 6.5 meter Magellan Telescopes, the Swope 1 meter telescope, and the *Swift* telescope.
[†] e–mail: svalenti@lcogt.net
[1] Note that we are not considering Type IIn nor Type IIb in this work, even though there are still several open issues on where these objects are situated in terms of SN II diversity.

a clear plateau phase, where the SN brightness stays nearly constant (in the optical) for roughly 100 days. The plateau phase is mainly powered by a moving hydrogen recombination front that travels through the hydrogen-rich material that is ejected and ionized during the explosion (Woosley et al. 1987). A prototypical example of a Type IIP SN is SN 1999em (Hamuy 2003). SNe IIL exhibit a linear decay that starts soon after peak brightness, They are more rare than SNe IIP and, because light curves of Type IIL SNe decline faster than light curves of Type IIP SNe, only a handful of SNe IIL have been followed for more that three months after peak brightness. Prototypical example of Type IIL SNe are SN 1979C and SN 1980K (see Filippenko 1997).

SNe IIL are on average more luminous than SNe IIP by ∼1.5 mag (Patat et al. 1993, 1994; Anderson et al. 2014; Sanders et al. 2014; Faran et al. 2014a). Spectroscopically, SNe IIL have on average redder continua and have higher oxygen to hydrogen ratio as compared to ordinary SNe IIP (Faran et al. 2014a). SNe IIL also exhibit higher expansion velocities at early times (Faran et al. 2014a), and less pronounced P-Cygni Hα profiles (Gutiérrez et al. 2014).

Given these differences, there is a general consensus that the progenitor stars of SNe IIL have a relatively small amount of hydrogen in their envelopes, while SNe IIP more likely originate from hydrogen-rich stars. It is not currently known whether the progenitors of SNe IIL gradually lose their hydrogen layer, creating a continuous class extending from SNe IIL to SN IIP, or if there is a specific mechanism that creates distinct classifications as has been previously suggested (Barbon, Ciatti & Rosino 1979; Patat et al. 1993).

This traditional classification scheme has been supported in recent compilations of SN II light curves by Arcavi et al. (2012) and Faran et al. (2014a). However, Anderson et al. (2014) and Sanders et al. (2014) have shown that the historical distinction between the two classes could be due to the small number of well observed SNe IIL. They have also suggested that the historical distinction between IIP and IIL, based on the presence of a plateau or a linear decay in the light curve, is insufficient for a complete mapping of SN II diversity. Anderson et al. (2014) suggested that if all SNe IIL are followed for a long enough time, they will exhibit, after the linear decay, a significant drop in their light curves. This would provide further evidence that IIP's and IIL's share the same underlying physics. However, the majority of SNe IIL recently presented by Anderson et al. (2014) and Sanders et al. (2014) have only been followed for a limited amount of time ($\lesssim$ 70-80 days from discovery).

Here we present detailed ultraviolet and optical broad-band photometry of the Type IIL SN 2013by, which covers the flux evolution of this object for over 150 days. Also presented are four visual-wavelength spectra and three near-IR (NIR) spectra. The data presented have been obtained by the Las Cumbres Observatory Global Telescope (LCOGT) network (Brown et al. 2013), the *Carnegie Supernova Project* (CSP; Hamuy et al. 2006), and with the UVOT camera aboard the *Swift* X-ray telescope (Burrows et al. 2005; Roming et al. 2005).

The organisation of this paper is as follows. In Section 2 we present the spectroscopic and photometric observations, and briefly characterise the data reduction process. Presented in Section 3 are the photometric data of SN 2013by, while in Section 4 we analyse the optical and NIR spectra of SN 2013by. In Section 5 we discuss the amount of ^{56}Ni produced in SN 2013by, and compare our results with the previous works of Hamuy (2003) and Spiro et al. (2014). Our results are summarized in Section 7.

2 OBSERVATIONS

SN 2013by was discovered by the Backyard Observatory Supernova Search (BOSS) on 2013 April 23.542 (UT), with coordinates at α=16h59m02s.43, δ=−60d11'41".8 (Parker et al. 2013). The SN is located 3″ West and 76″ North of the nucleus of the galaxy ESO 138−G10. The the NASA Extragalactic Database (NED)[2] distance, corrected for Local-group infall towards the Virgo cluster and assuming $H_0 = 73 \pm 5 \ \mathrm{km\,s^{-1}\,Mpc^{-1}}$, is D=14.8±1 Mpc (distance modulus = 30.84 ±0.15). This value is adopted throughout this work. The closest available pre-discovery limit is not stringent (on April 1.554 UT, Parker et al. 2013), but early spectroscopic and photometric follow-up are consistent with a supernova discovered a few days or less after explosion. In what follows we adopt April 21.5 (UT), i.e., JD = 2456404±2 days, as the explosion epoch. Spectroscopic confirmation as a young SN II came from both optical and NIR observations (Parker et al. 2013), along with a tentative classification as a Type IIL/IIn. Based on the light curve, SN 2013by, in the traditional schema, is a typical SN IIL (see Section 3). However X-ray emission has also been detected for SN 2013by with *Swift* (Margutti, Soderberg & Milisavljevic 2013), supporting the idea that SN 2013by may have experienced moderate interaction with circumstellar material (CSM) during early phases (see Section 4).

Photometric monitoring in $BVgri$ of SN 2013by with the LCOGT 1 m telescope network began on 2013 April 24 (UT), and continued every 2-3 nights (52 epochs of data were collected) for more than 150 days, well after the light curve settled onto the ^{56}Co decay tail. The LCOGT science images were reduced using a custom pipeline that performs point spread function (PSF) fitting and a low order polynomial fit to remove any background contamination (see Valenti et al. 2014). SN 2013by exploded close (but not coincident) to two point-like sources that are $\geqslant$ 2 magnitudes fainter than our last detection.

Additional imaging was obtained from *Swift* and the CSP. The *Swift* data (15 epochs) was reduced following the standard procedures described by Brown et al. (2009). While the PSF fitting technique gives a good result for ground-based data of SN 2013by, *Swift* magnitudes are computed using aperture photometry. By comparing initial *Swift* results with ground
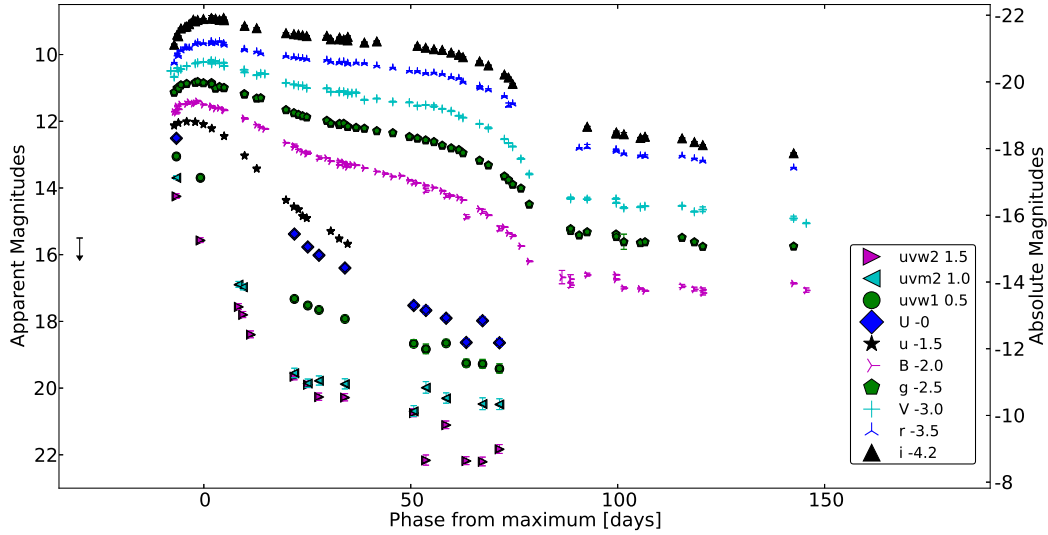
---

[2] http://ned.ipac.caltech.edu/

Figure 1. Ultraviolet and optical light curves of SN 2013by from observations obtained by LCOGT, CSP and *Swift*. From maximum light to ~ 65 days after maximum, SN 2013by experiences a nearly linear decline, with a decline rate per 50 days of $s50_V = 1.46$ mag. The V-band light curve then abruptly drops until a new, slow decline is established at $\sim +90$ days from maximum, presumably associated with the radioactive decay tail of $^{56}\mathrm{Co} \to {}^{56}\mathrm{Fe}$.

based measurements, host galaxy contamination was evident in the *Swift* data. This motivated a *Swift* Target of Opportunity program (PI S.Valenti) to re-image the field of SN 2013by one year after discovery in order to properly remove background host-galaxy contamination as prescribed by Brown et al. (2009).

The CSP obtained 17 epochs of science images using the SITe3 CCD camera along with a set of *ugriBV* filters attached to the Swope 1 m telescope located at Las Campanas Observatory (LCO). These images were reduced using the methodology described in Contreras et al. (2010) and Stritzinger et al. (2011). The CSP, LCOGT and *Swift* photometry are in good agreement except the *Swift V* band that is systematically 0.1 magnitude fainter that the LCOGT and CSP photometry. Given the good photometric coverage in V band with CSP and LCOGT data, we did not investigate this systematic difference further.

Four epochs of visual-wavelength spectra of SN 2013by were obtained with WifeS (Dopita et al. 2007) on the ANU 2.3m Telescope, and three epochs of NIR spectra with FIRE (Simcoe et al. 2013) on the Magellan 6.5 m Baade telescope (see Table A1). The optical spectra were reduced with PyWiFes as described by Childress et al. (2013), while the FIRE spectra were reduced using the IDL pipeline `Firehose`. The `Firehose` pipeline performed the following steps: flat fielding, wavelength calibration, sky subtraction, spectral tracing and extraction and flux calibration.

3 LIGHT CURVES

The multi-band light curves of SN 2013by are shown in Figure 1, while the corresponding photometric data are tabulated in Table A5. After inspecting the light curves, we see familiar features including a short rise (~ 10 days) to maximum, followed by a linear phase lasting 65 days (from maximum). After the linear phase, the light curve of SN 2013by shows a clear drop until it sits on the radioactive decay tail of $^{56}\mathrm{Co}$ to $^{56}\mathrm{Fe}$.

In order to determine which type of SN is SN 2013by, we compare its V-band light curve with templates presented by Faran et al. (2014a) (see left panel of Figure 2). SN 2013by lies in the middle of the SN IIL templates of Faran et al. (2014a). For completeness we also compare SN 2013by with the CSP sample of SNe II published by Anderson et al. (2014) (see right panel of Figure 2). The $s2$ parameter, used by Anderson et al. (2014) to quantify the slope of the plateau, is the V-band magnitude decline per 100 days measured in the second part of the plateau (see black line in left panel of Figure 2). Faran et al. (2014a) use a different parameter. Specifically, they use the magnitude decline in 50 days computed between maximum light and 50 days after explosion $(s50_V)$[3]. In order to avoid the proliferation of parameters to characterize SNe II, we adopt the $s50_V$ in this paper. Faran et al. (2014a) define all SNe II with $s50_V > 0.5$ mag as Type IIL events. The decline rate for SN 2013by is $s50_V = 1.46 \pm 0.06$ mag.

---

[3] The reader should be aware that since the rise time of SNe II is often not well defined and can takes several days from explosion, the $s50_V$ parameter is usually computed within a range of ~ 40–45 days.
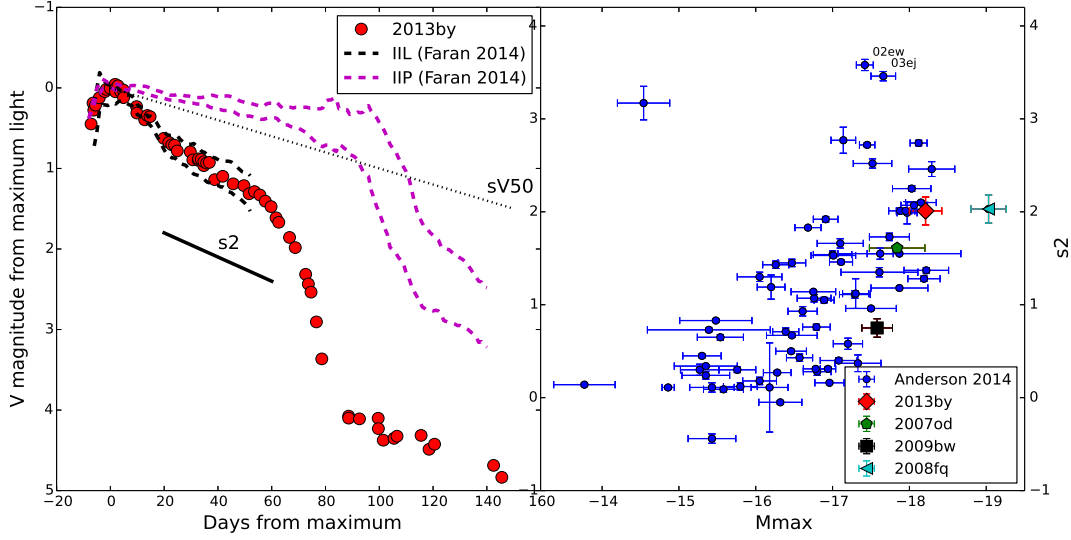
Figure 2. *left panel*: SN 2013by compared with template light curves from Faran et al. (2014b). The s2 parameter is the V-band magnitudes per 100 days of the second, shallower slope observed in the light curve as defined by Anderson et al. (2014). *right panel*: Absolute V-band magnitude of SN 2013by vs. s2, compared to objects from Anderson et al. (2014). SN 2009bw, SN 2007od and SN 2008fq have been also added for comparison.

In this schema SN 2013by should be labeled as a SN IIL. However, the presence of a drop in magnitude at the end of the hydrogen recombination phase is usually considered the defining feature of a SN IIP. Is the light curve drop-off in SN 2013by atypical for a SN IIL? To answer this question, we have compiled a large sample of SNe IIL from the literature, and systematically measured from their V-band light curves the parameter $s50_V$. Among these, we show a subset with $s50_V > 1.0$ (typically classified as SN IIL, as they are the fastest decliners) in Figure 3. We also show a handful of objects with $0.5 < s50_V < 1.0$ (orange symbols; SNe 2007od, 2007pk, 2009bw, 2009dd). If we follow the definition of Faran et al. (2014a), where SNe IIL decline with $s50_V > 0.5$, SN 2007od, SN 2007pk and SN 2009bw should also be classified as SNe IIL. These SNe II are as luminous as SNe IIL ($M_{IIL} = -17.44$ mag Li et al. 2011) ($M_V^{07od} = -17.4$ mag and $M_V^{09bw} = -17.2$ mag, Inserra et al. 2013). For comparison SNe IIP are fainter ($M_{IIP} = -15.66$ mag), (Li et al. 2011). These SNe have been studied in detail by Inserra et al. (2011) and Inserra et al. (2012). They identify high velocity Hα absorption in the spectra ($\sim$ 13,000-15,000 km s^{-1}) and suggest this is evidence for *moderate interaction* with CSM. Chugai, Chevalier & Utrobin (2007) have shown that the presence of high-velocity features in Type II SNe can be indeed interpreted as interaction between rapidly expanding SN ejecta and circumstellar material (CSM).

The SNe in Figure 3 are predominantly taken from Anderson et al. (2014) and Faran et al. (2014b), but also included are the historical Type IIL SN 1979C (Barbon, Ciatti & Rosino 1982) ($s50_V = 1.5$ mag) and SN 1980K (Barbon, Ciatti & Rosino 1982) ($s50_V = 2.1$ mag). Each of the SNe IIL plotted in Figure 3 show a linear decay up until $\sim$80–120 days after explosion, followed by a steep and rapid decline prior to reaching a secondary linear decline phase powered by radioactive decay. All SNe IIL that have been followed for more that 80 days from discovery show the drop in magnitude that is characteristic of SNe IIP. Based on observations of several SNe IIL, Anderson et al. (2014) noted a similar luminosity drop, however, their photometric coverage is not as dense as that presented here (particularly at late phases), so a drop could not be robustly demonstrated for most of their events. The light curve coverage of SN 2013by is such that it affords the best coverage of a late-time luminosity drop for a SN IIL. We also performed an extensive literature search for SNe IIL that do not show this light curve drop, and found that only SN 1979C may have been one such object. Actually also SN 1979C, as suggested by Anderson et al. (2014), may show a light curve drop around 50 days after explosion, though, if there, the drop would have occurred quite early and less pronounced than all the other cases. It is also worth mentioning (see Figure 3) that the light curve drop to the radioactive decay tail in SNe IIL occurs at $\sim$80–100 days (versus $\sim$ 100-140 days for SNe IIP, confirming the correlation between the slope of the plateau and plateau length previously reported by Anderson et al. (2014).

4   SPECTROSCOPY

The visual-wavelength spectra of SN 2013by are plotted in Figure 4, while the NIR spectra are shown in Figure 5. Also included in Figure 4 are comparison spectra of SN 2009bw and SN 2007od, which are found by the spectral classification tool GELATO (Harutyunyan et al. 2008) to best match the spectra of SN 2013by at 16 and 34 days after shock breakout. For the first spectrum of SN 2013by, GELATO find as best fit SN 1998S and several other SNe IIn. However the fit are poor,
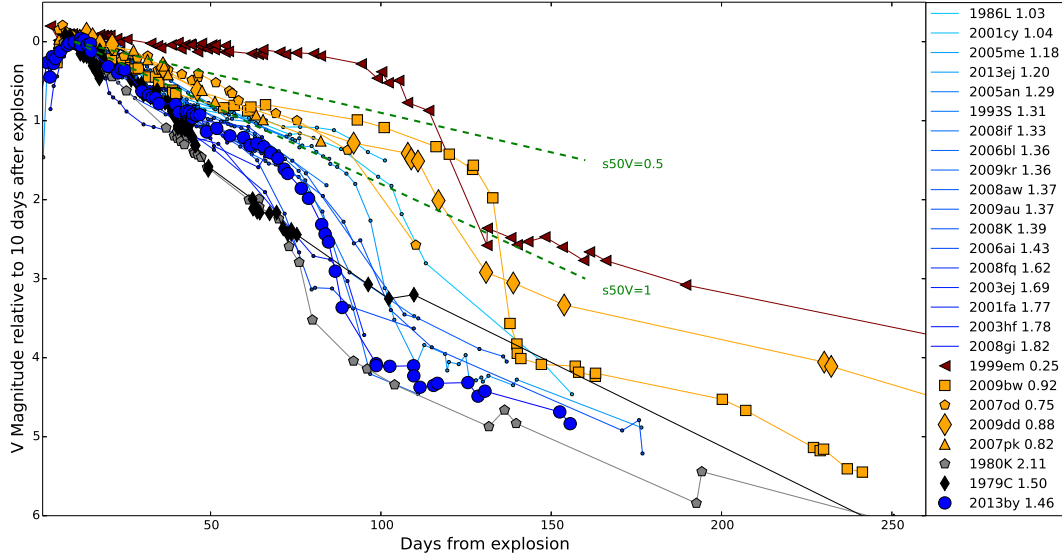
Figure 3. *V*-band light curves of a compilation of SNe II from the literature, along with SN 2013by. Each object is listed and color coded in the right panel along with its measured $s50_V$ parameter. We have chosen objects primarily with $s50_V > 1.0$ to highlight the fastest declining, SN IIL-like events. We have also included several objects with $0.5 < s50_V < 1.0$, which are plotted in orange and the prototype of Type IIP SN 1999em. Note that all of the high $s50_V$ objects have a steep drop-off from their linear 'plateau' phase at around $\sim$80-120 days, before the radioactive decay tail powers the light curve.

probably for the lack of SNe IIL spectra obtained at early phases. The spectrum of SN 2009bw obtained 4 days after shock breakout shows several similarities to SN 2013by, although the latter exhibits conspicuous He I λ5876 (see Fig. 4).

The first optical spectrum exhibits a blue continuum with the Balmer and the Paschen series clearly detected. Both He I and O III are detected in the first optical spectrum of SN 2013by. As the SN evolves the Balmer lines become more prominent and typical features of SNe II emerge including: Ca II (H&K $\lambda\lambda$3934, 3968 Å), Fe II (especially lines $\lambda\lambda$4924, 5018 and 5169 Å), Ti II (with many multiplets below 5400Å), O I λ7774 Å and the Ca II infrared triplet $\lambda\lambda$8498, 8542 and 8662 Å). The spectra at 16 and 34 days after explosion show several absorption features blueshifted with respect to photospheric Hα (marked as A, B and C in Figure 4b). While absorption feature A is consistent with Si II, absorption features B and C are probably due to Hα at 15000 km s^{-1} and 8000 km s^{-1}, respectively. As mentioned in Section 3, these high-velocity features have also been identified in SN 2009bw and SN 2007od (Inserra et al. 2011, 2012), and interpreted as having an origin related to the interaction between rapidly expanding SN ejecta and circumstellar material (CSM).

Besides the overall similarity with SN 2007od, SN 2013by does show one clear difference: the O I λ7774 absorption line in the spectrum of SN 2013by at 34 days after the explosion is quite prominent, while it is almost absent in the spectrum of SN 2007od. Faran et al. (2014a) have recently shown that oxygen seems to be more pronounced in SNe IIL than in SNe IIP and it can be interpreted as a sign of a more massive progenitor. However, oxygen should be used carefully as a progenitor tracer for SNe IIP. Maguire et al. (2012) and Jerkstrand et al. (2012) have shown that part of the oxygen visible in Type IIP SNe is synthesized soon after the explosion, while the rest is primordial oxygen that is mixed in the envelope during the evolution of the progenitor. Disentangling these contributions is not easy.

A comparison of the observed visual-wavelength spectrum at 34 days after the estimate shock breakout to our SYNOW fit in Figure 6. The spectrum has been reproduced with a black body temperature of 7200 K and a photospheric velocity of 7000 km s^{-1}. The following ions has been used in the synow spectrum: HI, Sr II, Sc II, Ca II, O I, Fe II, Na I, Ti II, and Si II. The SYNOW spectrum well reproduces the observed spectrum, except for the ratio of the Hα / Hβ. This is a well known problem related to the fact that SYNOW is based on the underlying assumption of local thermodynamical equilibrium (Dessart & Hillier 2010).

Plotted in Figure 5 are the 3 FIRE NIR spectra of SN 2013by compared to the spectra of other SNe II, including SNe 2002hh (Pozzo et al. 2006), 2012A (Tomasella et al. 2013) and 2012aw (Dall'Ora et al. 2014). Beside the asymmetric profile of Hydrogen lines, also visible in the optical spectra, the NIR spectra of SN 2013by are similar to those of other Type II SNe. Of particular interest is the last (+90d) FIRE spectrum of SN 2013by, which, to our knowledge, is one of only a handful of NIR late-time spectra published to date for a Type II SN, and the first of a Type IIL SN. Pozzo et al. (2006) published a large set of infrared spectra of SN 2002hh at late time.

SN 2002hh with a $s50_V = 0.27$ mag/50 days is a Type IIP SN. The first of their spectra (+137d) is shown in the comparison, and several of their line identifications have provided us with guidelines for our analysis of SN 2013by. Beside the Brackett series which is clearly visible in the spectrum of SN 2002hh in the range 16000-18000 Å, most of the other lines are also visible in the last spectrum of SN 2013by. This includes, e.g., Fe II, O I, Mg I, He I and Si I.

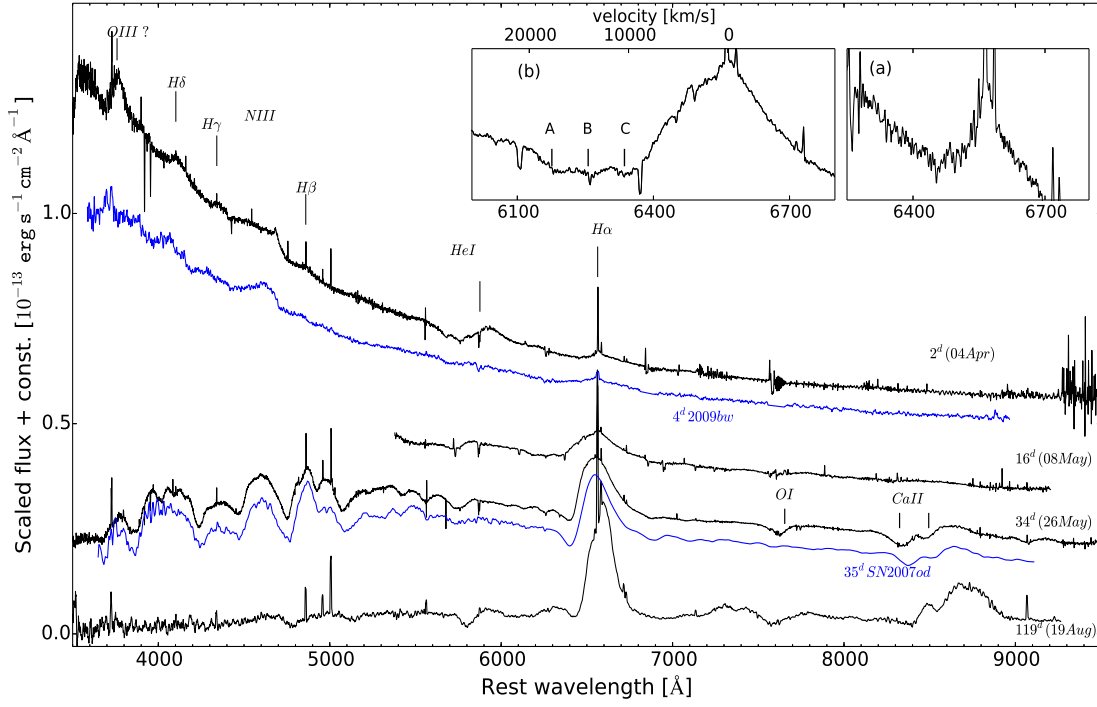**Figure 4.** Visual-wavelengths spectra of SN 2013by. Inset (a) and (b) show the region blue-wards of Hα, and highlight absorption features labeled as A, B, and C.
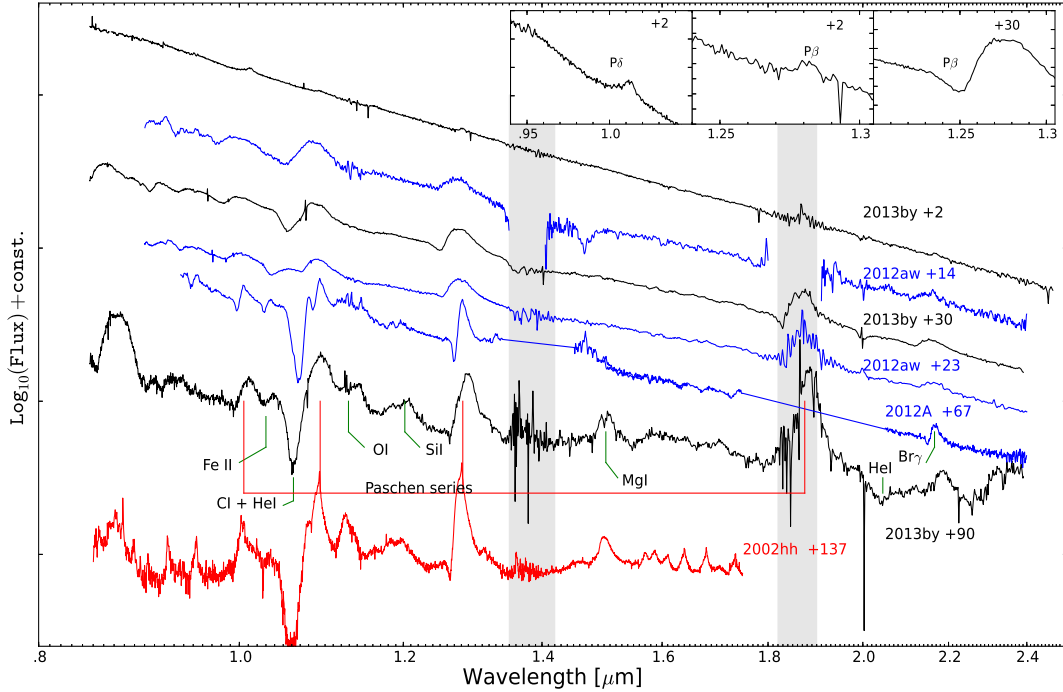

Figure 5. Infrared spectra of SN 2013by and several Type IIP SNe from the literature. The three inset panels show the asymmetric profile of Paschen lines in the spectra at 2 days ($P\beta$ and $P\delta$) and 30 days ($P\beta$) after the shock breakout.
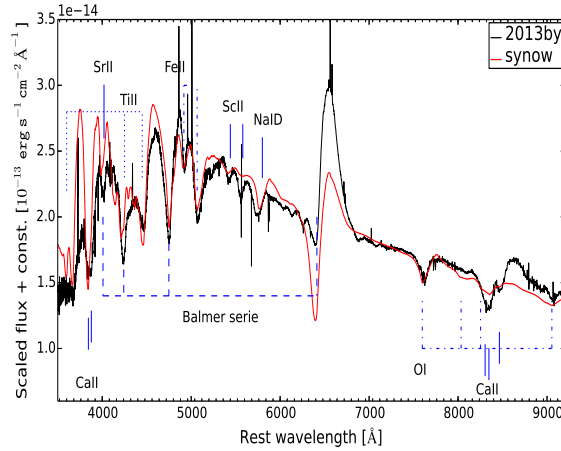
Figure 6. *Synow* fit of the spectrum of SN 2013by at 34 days after the estimate shock breakout.

The presence of O I at $\lambda 11290$ Å confirms the O I identification at optical wavelengths. As reported by Pozzo et al. (2006), this line is a Bowen resonance fluorescence line which requires the presence of microscopic mixing of hydrogen and oxygen in the ejecta to be excited. He I is also clearly visible at $\lambda 10830$ Å and $\lambda 20580$ Å. The presence of He I at this phase can be explained only if iron-group elements are mixed in the ejecta. The presence of O I and He I confirm that significant mixing has occurred within the ejecta. Mg I $\lambda 15030$ Å, is also clearly detected, while no sign of [Si I] $\lambda 16068$ Å is apparent.

5 ^{56}NI IN SNE IIP/IIL

Recent studies of SNe II have shown that the Type IIL objects are on average more luminous at peak brightness than Type IIP objects ($M_{IIL} = -17.44$ and $M_{IIP} = -15.66$, Li et al. 2011; see also Anderson et al. 2014; Faran et al. 2014a and Sanders et al. 2014). This is consistent with a scenario where the envelope of SNe IIL progenitors retains a much smaller amount of hydrogen than their SNe IIP counterparts. A massive hydrogen-rich envelope causes a slower release of energy and a fainter maximum luminosity due to its ionization and expansion during the SN explosion (Patat et al. 1994). A contribution to the extra luminosity of SNe IIL may also come from CSM interaction (see Section 6).

An alternative explanation for the higher luminosity observed in SNe IIL is a larger amount of ^{56}Ni synthesized during the explosion. The most appropriate way to estimate the ^{56}Ni content is by observing the supernova after ~ 100 days from explosion, when the ^{56}Co decay becomes the dominate source of energy that powers the broad-band emission. Unfortunately SNe IIL decline 4–5 magnitudes from peak and are often too faint to be observed at this phase. However, we were able to follow SN 2013by, and a few other SNe IIL for more than 100 days, recovering both the drop from the plateau typical of SNe IIP and the subsequent fall of the light curve onto the radioactive tail.

Using SN 1987A as reference, we estimated the amount of ^{56}Ni produced during the explosion using the method of Spiro et al. (2014). This method consists of comparing the pseudo-bolometric light curve of these objects with the pseudo-bolometric light curve of SN 1987A (integrated in the same bands) as soon as the SN fall onto the radioactive tail, such that

$$M_{SN}(Ni) = 0.075 \times \frac{L_{SN}}{L_{87A}} M_\odot. \tag{1}$$

Armed with this methodology, we measure the ^{56}Ni mass for 8 SNe II (see Table 1, recently published or with work in preparation). Hamuy (2003) and Spiro et al. (2014) presented a similar analysis for a sample of 27 and 17 SNe II, respectively. Figure 7 shows the relation between ^{56}Ni mass and the absolute V-band magnitude at 50 days from explosion for the 44 SNe (Hamuy 2003 and Spiro et al. 2014) and the 8 SNe from Table 1. For a sub-sample of these SNe, we were able to measure the $s50_V$ parameter. These SNe have been plotted in Figure 7 with different colors depending on their $s50_V$ values (bluer points for larger slopes, red points for lower slopes).

Hamuy (2003) have shown a clear relation between ^{56}Ni mass and the absolute V-band magnitude (at 50 days from explosion). Spiro et al. (2014) confirmed that faint SNe IIP also follow the same relation. Even though the number of SNe IIL with a ^{56}Ni estimate from the radioactive tail is small, these objects seem to follow the same relations. However, part of the scatter in this relation seems to be related to the $s50_V$ parameter. Blue points (SNe IIL) sit slightly brighter than the general trend for a given ^{56}Ni mass.
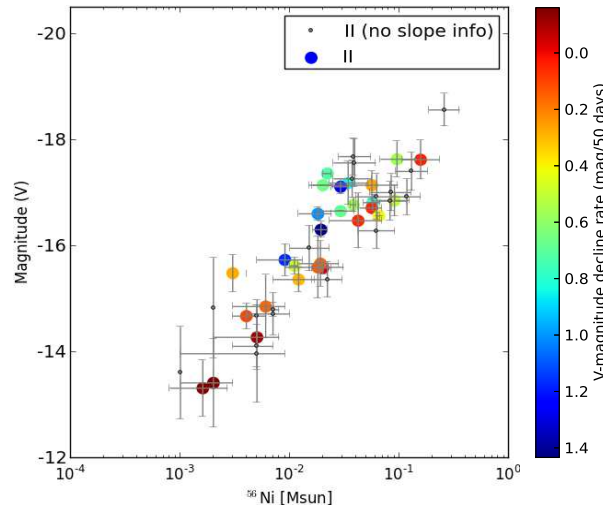
Figure 7. Absolute *V*-band magnitude at 50 days from explosion versus ^{56}Ni mass for a sample of SNe II. SNe IIL (blue points) cluster on the top-left side of the relation. The data are from Hamuy (2003), Spiro et al. (2014) and this work.

6   SNE IIL AND CSM INTERACTION

We have shown in section 3 and section 4 that, SN 2013by is similar to the class of *moderately interacting* Type II SNe. X-ray emission has also been detected for SN 2013by with *Swift* (Margutti, Soderberg & Milisavljevic 2013). They measure a 0.3-1.0 keV count-rate of 2.1 ± 0.7 cps, that assuming a simple power-law spectra model with photon index Gamma =2, translate in a flux of 1.1e-13 erg/s/cm2 (.3-10 keV).

This raises several questions: Are all Type IIL SNe interacting with CSM? Do all *moderately interacting* Type II SNe decline like SNe IIL? It is not straight forward to generalize, but if SNe IIL are coming from progenitors that lost most of their hydrogen envelope during pre-SN evolution, it is more likely that these SNe (more than Type IIP SNe) will show CSM interaction. Unfortunately, for most of the objects we do not have enough information to answer these questions. It is indeed difficult to clearly separate between interacting and not interactive SNe II.

At very early phases SNe IIP/IIL may be very similar to SNe IIn since the SN ejecta has not yet had time to reach and shock the CSM. SN 2008fq is a clear example of a SN II that shows sign of interaction at very early phases. It has been considered to be a SN IIn by Taddia et al. (2013) because of the clear detection of narrow lines in its spectra before maximum, while Faran et al. (2014a) include this SN in their sample of SNe IIL since no narrow lines are visible after maximum light. Photometrically SN 2008fq and SN 2013by have similar slopes after maximum even though SN 2008fq is one magnitude brighter than SN 2013by (see right panel of Figure 2 and Figure 8). Unfortunately both light curves from Faran et al. (2014a) and Taddia et al. (2013) stop at ∼ 60 days, before the drop from the plateau would have occurred. Plotted in Figure 8 (left panel) are the absolute *V*-band magnitude light curve of SN2008fq and three other SNe that (right, top panel) show signs of interaction with CSM at early phases.

7   CONCLUSIONS

We have presented UV and optical broad-band photometry for the Type IIL SN 2013by ranging up to 150 days after explosion. Our extended and dense photometric coverage confirms that all SNe IIL show a similar drop in the light curve down to the radioactive tail as is seen in SNe IIP, but at an earlier stage. If SNe IIL are followed for more than 80-100 days, they show that SNe IIP and IIL share similar underling physics, supporting the idea that the separation in two classes is purely nominal. Only a handful of objects that decline as fast as SNe IIL do not show the drop from the plateau, suggesting that their light curves may be powered (also) by a different source of energy (different than recombination). We suggest that the drop from the plateau (instead of the slope) should be use as a more physical parameter to distinguish different types of SNe II.

We have also presented visual-wavelength and NIR spectra of SN 2013by, and have made a detailed comparison to similar data of other SNe II. The visual-wavelength spectra suggest that SN 2013by has experienced a moderate amount of interaction between its rapidly expanding ejecta and its CSM for more than one month after explosion. Several SNe II show evidence of interaction with the CSM at early phases. Most of these objects are moderately luminous and they show a fast *V* light curve decline after maximum similar to SNe IIL. A late (+90d relative to peak) NIR spectrum of SN 2013by exhibits similarities to a NIR spectrum of the Type IIP SN 2002hh. This comparison strengthens the similarity between Type IIP and IIL SNe suggesting that strong mixing occurs in the progenitors of both varieties.

We also investigate whether or not SNe IIL are on average more luminous than SNe IIP, and if so, if this is related to the amount of ^{56}Ni synthesized during the explosion. We use the magnitude vs. ^{56}Ni relations introduced by Hamuy (2003)
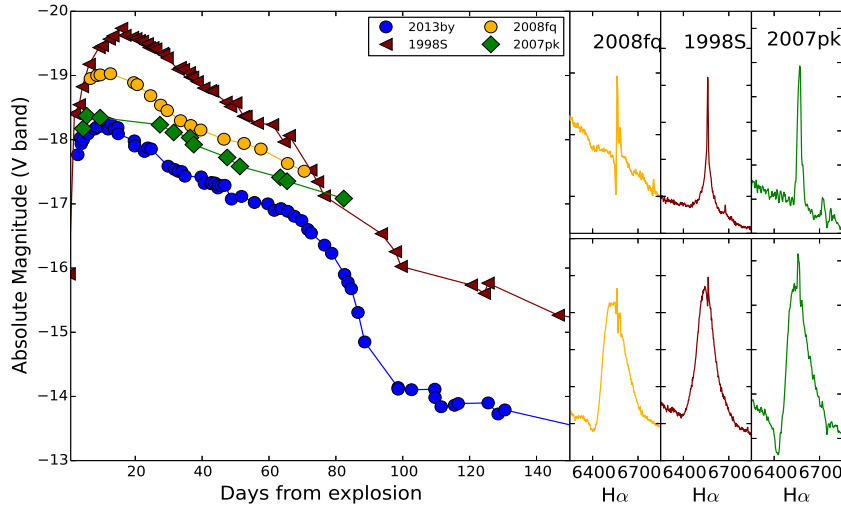
Figure 8. *(left panel)* V-band absolute magnitude light curve of SNe II that show at early phases signs of interaction with CSM; *(right panel)* Hα profiles soon after discovery (top) and at the end of the plateau phase (bottom) for three SNe IIP/L-IIn.

Table 1. Main parameters for Type IIL and IIP SNe (added to the previous works)

Supernova	Nickel	M_V^a	M_{V50}^b	Distance modulus^c	$E(B-V)_{host}$	$E(B-V)_{MW}^d$	Explosion epoch	Ref^e.
SN 2003hn	0.038 (002)	−17.40 (14)	−16.78 (03)	32.25 (12)	0.173	0.014	2452870.0 (4)	1
SN 2009kr	0.009 (004)	−16.82 (30)	−15.74 (08)	32.09 (50)	0.0	0.077	2455140.5 (2)	2
SN 2013by	0.029 (005)	−18.21 (14)	−17.12 (11)	30.85 (15)	0.0	0.195	2456404.0 (2)	3
SN 2013ej	0.018 (006)	−17.27 (13)	−16.61 (10)	29.79 (02)	0.0	0.061	2456497.4 (2)	4
SN 2013fs	0.057 (006)	−17.71 (15)	−16.82 (04)	33.5 (15)	0.0	0.035	2456571.2 (1)	5
SN 2014G	0.019 (003)	−17.46 (15)	−16.32 (08)	31.83 (02)	0.0	0.012	2456668.3 (1)	6
SN 2012A	0.011 (001)	−16.28 (16)	−15.63 (14)	29.96 (15)	0.012	0.024	2455932.5 (2)	7
SN 2012aw	0.056 (013)	−16.92 (10)	−16.72 (10)	29.96 (02)	0.028	0.058	2456002.5 (1)	8

^{a} Absolute magnitude at maximum. ^{b} Absolute magnitude at 50 days after explosion. ^{c} From NED, corrected for Local-Group infall onto the Virgo cluster and assuming $H_0 = 73 \pm 5$ km s^{-1} Mpc^{-1}. ^{d} Schlegel, Finkbeiner & Davis (1998). ^{e} References:
1=Krisciunas et al. (2009); 2=Fraser et al. (2009), Elias-Rosa et al. (2011); 3= this work, 4= Valenti et al. (2014); 5= Trematerra et al in prep ; 6= Yaron et al in prep.; 7= Tomasella et al. (2013) ; 8= Dall'Ora et al. (2014).

and Spiro et al. (2014), adding as extra information the slope in V-band light curve ($s50_V$). We find that SNe IIL broadly follow these relations, but for a similar amount of ^{56}Ni produced during the explosion, SNe IIL are on average brighter than SNe IIP. This is in agreement with the idea that SNe II with a larger ejected mass, have a slower release of energy and a fainter maximum luminosity due to its ionization and expansion during the SN explosion.

REFERENCES

Anderson J. P. et al., 2014, The Astrophysical Journal, 786, 67
Arcavi I. et al., 2012, The Astrophysical Journal, 756, L30
Barbon ., Ciatti ., Rosino ., 1979, Astronomy and Astrophysics, 72, 287
Barbon, 1982, Astronomy and Astrophysics, 116, 35

Brown P. J. et al., 2009, The Astronomical Journal, 137, 4517

Brown T. M. et al., 2013, Publications of the Astronomical Society of the Pacific, 125, 1031

Burrows D. N. et al., 2005, Space Science Reviews, 120, 165

Childress M. J., Vogt F. P. A., Nielsen J., Sharp R. G., 2013, Astrophysics and Space Science, 349, 617

Chugai N. N., 2001, Monthly Notices of the Royal Astronomical Society, 326, 1448

Chugai N. N., Chevalier R. A., Utrobin V. P., 2007, The Astrophysical Journal, 662, 1136

Contreras C. et al., 2010, The Astronomical Journal, 139, 519

Dall'Ora M. et al., 2014, The Astrophysical Journal, 787, 139

Dessart L., Hillier D. J., 2010, Monthly Notices of the Royal Astronomical Society, 410, 1739

Dopita M., Hart J., McGregor P., Oates P., Bloxham G., Jones D., 2007, Astrophysics and Space Science, 310, 255

Elias-Rosa N. et al., 2011, The Astrophysical Journal, 742, 6

Faran, T., Poznanski, D., Filippenko, A. V., et al. 2014, Monthly Notices of the Royal Astronomical Society, 445, 554

Faran, T., Poznanski, D., Filippenko, A. V., et al. 2014, Monthly Notices of the Royal Astronomical Society, 442, 844

Fassia A. et al., 2000, Monthly Notices of the Royal Astronomical Society, 318, 1093

Filippenko A. V., 1997, Annual Review of Astronomy and Astrophysics, 35, 309

Fraser M. et al., 2009, The Astrophysical Journal Letters, 714, L280

Gutiérrez C. P. et al., 2014, The Astrophysical Journal, 786, L15

Hamuy M., 2003, The Astrophysical Journal, 582, 905

Hamuy M. et al., 2006, Publications of the Astronomical Society of the Pacific, 118, 2

Harutyunyan A. H. et al., 2008, Astronomy and Astrophysics, 488, 383

Inserra C. et al., 2013, Astronomy & Astrophysics, 555, A142

Inserra C. et al., 2011, Monthly Notices of the Royal Astronomical Society, 417, 261

Inserra C. et al., 2012, Monthly Notices of the Royal Astronomical Society, 422, 1122

Jerkstrand A., Fransson C., Maguire K., Smartt S., Ergon M., Spyromilio J., 2012, Astronomy and Astrophysics, 546, 28

Krisciunas K. et al., 2009, The Astronomical Journal, 137, 34

Li W. et al., 2011, Monthly Notices of the Royal Astronomical Society, 412, 1441

Maguire K. et al., 2012, Monthly Notices of the Royal Astronomical Society, 420, 3451

Margutti ., Soderberg ., Milisavljevic ., 2013, The Astronomer's Telegram

Parker . et al., 2013, Central Bureau Electronic Telegrams

Patat F., Barbon R., Cappellaro E., Turatto M., 1994, Astronomy and Astrophysics (ISSN 0004-6361), 282, 731

Patat ., Barbon ., Cappellaro ., Turatto ., 1993, Astronomy and Astrophysics Supplement Series (ISSN 0365-0138), 98, 443

Pozzo M. et al., 2006, Monthly Notices of the Royal Astronomical Society, 368, 1169

Roming P. W. A. et al., 2005, Space Science Reviews, 120, 95

Sanders . et al., 2014, eprint arXiv:1404.2004

Schlegel D. J., Finkbeiner D. P., Davis M., 1998, The Astrophysical Journal, 500, 525

Simcoe R. A. et al., 2013, Publications of the Astronomical Society of the Pacific, 125, 270

Spiro S. et al., 2014, Monthly Notices of the Royal Astronomical Society, 439, 2873

Stritzinger M. D. et al., 2011, The Astronomical Journal, 142, 156

Taddia F. et al., 2013, Astronomy & Astrophysics, 555, A10

Tomasella L. et al., 2013, Monthly Notices of the Royal Astronomical Society, -1, 25

Valenti S. et al., 2014, Monthly Notices of the Royal Astronomical Society: Letters, 438, L101

Woosley S. E., Pinto P. A., Martin P. G., Weaver T. A., 1987, The Astrophysical Journal, 318, 664

APPENDIX A: TABLES

Table A1. Journal of spectroscopic observations.

Date	Telescope	JD −2,400,000 (days)	Phase[a] (days)	Instrument	Range (Å)	Resolution FWHM[b] (Å)
2013 Apr 24	Magellan	56406.88	1.8	FIRE	9000-25000	4
2013 Apr 24	ANU 2.3m	56407.00	2.0	WifeS	3200-10000	1
2013 May 08	ANU 2.3m	56421.00	16.0	WifeS	3200-10000	1
2013 May 22	Magellan	56435.01	30.0	FIRE	9000-25000	4
2013 May 26	ANU 2.3m	56421.000	34.0	WifeS	3200-10000	1
2013 Jul 29	Magellan	56503.01	98.0	FIRE	9000-25000	4
2013 May 26	ANU 2.3m	56524.000	119.0	WifeS	3200-10000	1

[a] Relative to the date of the estimate shock breakout (SN 2013by, JD = 2456405.0; SN 2013ej, JD = 2456497.45).

[b] FWHM of night-sky emission lines.

Table A2. Photometric Data (Complete table available in the online version of the paper. Errors include photometry errors and errors on the nightly zero point.)

Date	JD	mag^a	Filter	telescope^b	Date	JD	mag	Filter	telescope ^{a}
2013-04-24	2456407.372	12.763 0.070	uw2	Swift	2013-06-04	2456448.092	16.409 0.070	U	Swift
2013-04-30	2456413.176	14.084 0.073	uw2	Swift	2013-06-21	2456464.719	17.533 0.095	U	Swift
2013-05-09	2456422.406	16.076 0.089	uw2	Swift	2013-06-24	2456467.659	17.680 0.114	U	Swift
2013-05-10	2456423.475	16.314 0.092	uw2	Swift	2013-06-29	2456472.541	17.914 0.094	U	Swift
2013-05-12	2456425.345	16.908 0.102	uw2	Swift	2013-07-03	2456477.411	18.643 0.106	U	Swift
2013-05-23	2456435.884	18.169 0.103	uw2	Swift	2013-07-07	2456481.348	17.990 0.105	U	Swift
2013-05-26	2456439.121	18.410 0.095	uw2	Swift	2013-07-11	2456485.430	18.652 0.120	U	Swift
2013-05-29	2456441.826	18.778 0.109	uw2	Swift	2013-04-24	2456407.370	13.753 0.047	B	Swift
2013-06-04	2456448.096	18.794 0.108	uw2	Swift	2013-05-23	2456435.882	14.753 0.048	B	Swift
2013-06-21	2456464.722	19.259 0.119	uw2	Swift	2013-05-26	2456439.119	14.966 0.047	B	Swift
2013-06-24	2456467.661	20.678 0.153	uw2	Swift	2013-05-29	2456441.823	15.112 0.049	B	Swift
2013-06-29	2456472.545	19.620 0.114	uw2	Swift	2013-06-04	2456448.093	15.332 0.050	B	Swift
2013-07-03	2456477.415	20.695 0.119	uw2	Swift	2013-06-21	2456464.720	15.847 0.054	B	Swift
2013-07-07	2456481.351	20.720 0.131	uw2	Swift	2013-06-24	2456467.660	16.088 0.062	B	Swift
2013-07-11	2456485.433	20.346 0.132	uw2	Swift	2013-06-29	2456472.542	16.249 0.055	B	Swift
2013-04-24	2456407.377	12.707 0.059	um2	Swift	2013-07-03	2456477.412	16.880 0.062	B	Swift
2013-05-09	2456422.411	15.909 0.088	um2	Swift	2013-07-07	2456481.349	16.722 0.064	B	Swift
2013-05-10	2456423.480	15.984 0.089	um2	Swift	2013-07-11	2456485.431	17.231 0.074	B	Swift
2013-05-23	2456435.888	18.566 0.142	um2	Swift	2013-04-24	2456406.830	13.732 0.008	B	CSP
2013-05-26	2456439.124	18.873 0.124	um2	Swift	2013-04-25	2456407.850	13.653 0.006	B	CSP
2013-05-29	2456441.830	18.792 0.138	um2	Swift	2013-04-27	2456409.860	13.496 0.005	B	CSP
2013-06-04	2456448.100	18.892 0.152	um2	Swift	2013-04-29	2456411.920	13.468 0.005	B	CSP
2013-06-21	2456464.726	19.709 0.163	um2	Swift	2013-05-01	2456413.910	13.516 0.013	B	CSP
2013-06-24	2456467.664	18.999 0.174	um2	Swift	2013-05-03	2456415.900	13.559 0.005	B	CSP
2013-06-29	2456472.550	19.318 0.155	um2	Swift	2013-05-06	2456418.900	13.684 0.005	B	CSP
2013-07-07	2456481.355	19.489 0.177	um2	Swift	2013-05-11	2456423.850	13.939 0.006	B	CSP
2013-07-11	2456485.437	19.502 0.162	um2	Swift	2013-05-14	2456426.770	14.118 0.005	B	CSP
2013-04-24	2456407.367	12.566 0.057	uw1	Swift	2013-05-21	2456433.840	14.660 0.006	B	CSP
2013-04-30	2456413.183	13.206 0.058	uw1	Swift	2013-05-23	2456435.750	14.784 0.006	B	CSP
2013-05-23	2456435.879	16.837 0.087	uw1	Swift	2013-05-24	2456436.850	14.863 0.005	B	CSP
2013-05-26	2456439.117	17.034 0.080	uw1	Swift	2013-05-25	2456437.870	14.930 0.006	B	CSP
2013-05-29	2456441.821	17.167 0.091	uw1	Swift	2013-05-26	2456438.870	14.984 0.005	B	CSP
2013-06-04	2456448.090	17.437 0.096	uw1	Swift	2013-06-01	2456444.678	15.210 0.006	B	CSP
2013-06-21	2456464.718	18.182 0.119	uw1	Swift	2013-06-03	2456446.685	15.326 0.011	B	CSP
2013-06-24	2456467.658	18.344 0.144	uw1	Swift	2013-06-05	2456448.732	15.381 0.009	B	CSP
2013-06-29	2456472.539	18.167 0.108	uw1	Swift	2013-04-25	2456407.560	13.563 0.021	B	1m0-10
2013-07-03	2456477.409	18.769 0.117	uw1	Swift	2013-04-25	2456408.459	13.507 0.006	B	1m0-10
2013-07-07	2456481.347	18.790 0.132	uw1	Swift	2013-04-27	2456410.459	13.436 0.011	B	1m0-10
2013-07-11	2456485.428	18.931 0.138	uw1	Swift	2013-04-28	2456411.459	13.482 0.017	B	1m0-10
2013-04-24	2456406.830	13.638 0.018	u	CSP	2013-04-30	2456412.500	13.411 0.019	B	1m0-10
2013-04-25	2456407.850	13.561 0.009	u	CSP	2013-05-03	2456415.845	13.586 0.007	B	1m0-5
2013-04-27	2456409.850	13.520 0.008	u	CSP	2013-05-04	2456416.801	13.632 0.007	B	1m0-5
2013-04-29	2456411.920	13.531 0.007	u	CSP	2013-05-05	2456417.779	13.613 0.012	B	1m0-4
2013-05-01	2456413.900	13.601 0.011	u	CSP	2013-05-05	2456418.778	13.667 0.007	B	1m0-4
2013-05-03	2456415.910	13.726 0.006	u	CSP	2013-05-11	2456423.738	13.919 0.007	B	1m0-9
2013-05-06	2456418.910	13.956 0.008	u	CSP	2013-05-15	2456427.738	14.197 0.015	B	1m0-9
2013-05-11	2456423.850	14.540 0.008	u	CSP	2013-05-16	2456428.749	14.242 0.009	B	1m0-9
2013-05-14	2456426.780	14.931 0.009	u	CSP	2013-05-31	2456443.706	15.113 0.005	B	1m0-9
2013-05-21	2456433.860	15.873 0.014	u	CSP	2013-06-03	2456446.786	15.219 0.029	B	1m0-4
2013-05-23	2456435.770	16.074 0.011	u	CSP	2013-06-04	2456447.786	15.241 0.011	B	1m0-4
2013-05-24	2456436.870	16.154 0.012	u	CSP	2013-06-05	2456448.786	15.298 0.002	B	1m0-4
2013-05-25	2456437.870	16.354 0.013	u	CSP	2013-06-06	2456449.785	15.315 0.009	B	1m0-4
2013-05-26	2456438.860	16.414 0.012	u	CSP	2013-06-07	2456450.788	15.331 0.011	B	1m0-4
2013-06-01	2456444.673	16.803 0.012	u	CSP	2013-06-09	2456452.787	15.417 0.011	B	1m0-4
2013-06-03	2456446.694	17.029 0.021	u	CSP	2013-06-12	2456455.786	15.522 0.000	B	1m0-4
2013-06-05	2456448.742	17.186 0.025	u	CSP	2013-06-14	2456457.791	15.588 0.019	B	1m0-4
2013-04-24	2456407.369	12.521 0.053	U	Swift	2013-06-16	2456459.658	15.674 0.010	B	1m0-9
2013-05-23	2456435.881	15.392 0.060	U	Swift	2013-06-18	2456461.670	15.648 0.008	B	1m0-4
2013-05-26	2456439.118	15.780 0.059	U	Swift	2013-06-20	2456463.657	15.789 0.016	B	1m0-4
2013-05-29	2456441.822	16.026 0.066	U	Swift	2013-06-22	2456465.592	15.866 0.004	B	1m0-4

^{a} (a): Data has not been corrected for extinction; (b): *Swift* Telescope; CSP (Las Campanas, Chile); 1m0-08 (McDonald observatory, USA); 1m0-10, 1m0-12, 1m0-13 (Sutherland, South Africa), 1m0-04, 1m0-05, 1m0-09 (Cerro Tololo, Chile); 1m0-03, 1m0-11 (Siding Spring, Australia).

Table A3. Photometric Data

Date	JD	mag	Filter	telescope	Date	JD	mag	Filter	telescope [a]
2013-06-24	2456467.592	15.941 0.014	B	1m0-4	2013-07-19	2456492.626	17.005 0.003	g	1m0-4
2013-06-26	2456469.592	16.005 0.009	B	1m0-4	2013-07-29	2456502.622	17.794 0.041	g	1m0-4
2013-06-28	2456471.592	16.100 0.011	B	1m0-4	2013-07-29	2456502.626	17.740 0.050	g	1m0-9
2013-06-30	2456473.758	16.248 0.023	B	1m0-5	2013-07-31	2456504.692	17.929 0.031	g	1m0-9
2013-07-02	2456475.616	16.300 0.004	B	1m0-4	2013-08-02	2456506.625	17.833 0.025	g	1m0-5
2013-07-03	2456476.616	16.376 0.005	B	1m0-4	2013-08-09	2456513.600	17.901 0.022	g	1m0-9
2013-07-07	2456480.616	16.637 0.002	B	1m0-4	2013-08-09	2456513.662	17.975 0.023	g	1m0-4
2013-07-09	2456482.745	16.830 0.007	B	1m0-5	2013-08-10	2456515.492	18.133 0.227	g	1m0-4
2013-07-13	2456486.612	17.186 0.012	B	1m0-4	2013-08-14	2456519.480	18.158 0.003	g	1m0-9
2013-07-14	2456487.612	17.363 0.002	B	1m0-4	2013-08-16	2456520.594	18.133 0.023	g	1m0-5
2013-07-15	2456488.612	17.445 0.032	B	1m0-4	2013-08-25	2456529.548	18.000 0.017	g	1m0-9
2013-07-17	2456490.612	17.754 0.007	B	1m0-4	2013-08-28	2456532.523	18.134 0.008	g	1m0-5
2013-07-19	2456492.620	18.213 0.015	B	1m0-4	2013-08-30	2456534.553	18.269 0.012	g	1m0-4
2013-07-27	2456500.537	18.692 0.200	B	1m0-4	2013-09-21	2456556.514	18.263 0.019	g	1m0-4
2013-07-29	2456502.612	18.745 0.126	B	1m0-4	2013-04-24	2456406.820	13.649 0.009	g	CSP
2013-07-29	2456502.617	18.927 0.077	B	1m0-9	2013-04-25	2456407.850	13.539 0.006	g	CSP
2013-08-02	2456506.616	18.618 0.044	B	1m0-5	2013-04-27	2456409.850	13.387 0.005	g	CSP
2013-08-09	2456513.586	18.616 0.006	B	1m0-9	2013-04-29	2456411.920	13.351 0.005	g	CSP
2013-08-09	2456513.650	18.755 0.019	B	1m0-4	2013-05-01	2456413.900	13.363 0.010	g	CSP
2013-08-10	2456515.480	19.015 0.031	B	1m0-4	2013-05-03	2456415.900	13.399 0.005	g	CSP
2013-08-14	2456519.468	19.033 0.017	B	1m0-9	2013-05-06	2456418.910	13.510 0.005	g	CSP
2013-08-16	2456520.582	19.101 0.017	B	1m0-5	2013-05-11	2456423.850	13.703 0.005	g	CSP
2013-08-25	2456529.538	18.959 0.048	B	1m0-9	2013-05-14	2456426.770	13.824 0.005	g	CSP
2013-08-28	2456532.513	19.051 0.056	B	1m0-5	2013-05-21	2456433.850	14.171 0.005	g	CSP
2013-08-30	2456534.541	19.061 0.042	B	1m0-4	2013-05-23	2456435.760	14.262 0.006	g	CSP
2013-08-30	2456534.593	19.160 0.067	B	1m0-9	2013-05-24	2456436.860	14.313 0.005	g	CSP
2013-09-21	2456556.503	18.875 0.018	B	1m0-4	2013-05-25	2456437.860	14.355 0.005	g	CSP
2013-09-24	2456559.564	19.083 0.065	B	1m0-4	2013-05-26	2456438.860	14.390 0.005	g	CSP
2013-04-25	2456407.545	13.519 0.015	g	1m0-10	2013-06-01	2456444.666	14.579 0.005	g	CSP
2013-04-25	2456408.462	13.428 0.009	g	1m0-10	2013-06-03	2456446.688	14.617 0.009	g	CSP
2013-04-30	2456412.503	13.329 0.008	g	1m0-10	2013-06-05	2456448.735	14.675 0.009	g	CSP
2013-05-03	2456415.783	13.379 0.028	g	1m0-4	2013-04-24	2456406.830	13.683 0.009	V	CSP
2013-05-03	2456415.856	13.361 0.003	g	1m0-5	2013-04-25	2456407.850	13.512 0.006	V	CSP
2013-05-04	2456416.813	13.527 0.007	g	1m0-5	2013-04-27	2456409.860	13.359 0.005	V	CSP
2013-05-05	2456417.783	13.478 0.004	g	1m0-4	2013-04-29	2456411.920	13.283 0.005	V	CSP
2013-05-06	2456418.783	13.510 0.002	g	1m0-4	2013-05-01	2456413.900	13.238 0.008	V	CSP
2013-05-11	2456423.746	13.694 0.027	g	1m0-9	2013-05-03	2456415.900	13.284 0.005	V	CSP
2013-05-15	2456427.745	13.815 0.011	g	1m0-9	2013-05-06	2456418.900	13.357 0.006	V	CSP
2013-05-31	2456443.715	14.492 0.007	g	1m0-9	2013-05-11	2456423.850	13.548 0.005	V	CSP
2013-06-03	2456446.791	14.583 0.005	g	1m0-4	2013-05-14	2456426.770	13.632 0.005	V	CSP
2013-06-04	2456447.791	14.581 0.009	g	1m0-4	2013-05-21	2456433.850	13.862 0.005	V	CSP
2013-06-05	2456448.792	14.673 0.006	g	1m0-4	2013-05-23	2456435.760	13.912 0.006	V	CSP
2013-06-07	2456450.796	14.703 0.025	g	1m0-4	2013-05-24	2456436.850	13.942 0.005	V	CSP
2013-06-09	2456452.792	14.729 0.000	g	1m0-4	2013-05-25	2456437.870	13.946 0.005	V	CSP
2013-06-12	2456455.792	14.802 0.004	g	1m0-4	2013-05-26	2456438.870	14.018 0.005	V	CSP
2013-06-16	2456459.666	14.862 0.026	g	1m0-9	2013-06-01	2456444.677	14.129 0.005	V	CSP
2013-06-20	2456463.666	14.977 0.007	g	1m0-4	2013-06-03	2456446.686	14.136 0.009	V	CSP
2013-06-22	2456465.598	15.025 0.005	g	1m0-4	2013-06-05	2456448.734	14.201 0.006	V	CSP
2013-06-24	2456467.598	15.079 0.002	g	1m0-4	2013-04-25	2456407.566	13.423 0.007	V	1m0-10
2013-06-26	2456469.598	15.129 0.013	g	1m0-4	2013-04-25	2456408.461	13.449 0.004	V	1m0-10
2013-06-28	2456471.598	15.237 0.010	g	1m0-4	2013-04-30	2456412.502	13.254 0.005	V	1m0-10
2013-06-30	2456473.763	15.317 0.021	g	1m0-5	2013-05-03	2456415.781	13.191 0.024	V	1m0-4
2013-07-02	2456475.622	15.369 0.002	g	1m0-4	2013-05-03	2456415.851	13.250 0.020	V	1m0-5
2013-07-03	2456476.622	15.464 0.009	g	1m0-4	2013-05-04	2456416.809	13.209 0.004	V	1m0-5
2013-07-07	2456480.622	15.688 0.013	g	1m0-4	2013-05-05	2456417.781	13.277 0.001	V	1m0-4
2013-07-09	2456482.751	15.831 0.002	g	1m0-5	2013-05-06	2456418.781	13.261 0.010	V	1m0-4
2013-07-13	2456486.619	16.161 0.019	g	1m0-4	2013-05-11	2456423.742	13.468 0.005	V	1m0-9
2013-07-14	2456487.618	16.272 0.005	g	1m0-4	2013-05-15	2456427.742	13.578 0.010	V	1m0-9
2013-07-15	2456488.619	16.407 0.011	g	1m0-4	2013-05-16	2456428.754	13.593 0.005	V	1m0-9
2013-07-17	2456490.622	16.523 0.038	g	1m0-4	2013-05-31	2456443.712	14.029 0.008	V	1m0-9

[a] *Swift* Telescope; CSP (Las Campanas, Chile); 1m0-08 (McDonald observatory, USA); 1m0-10, 1m0-12, 1m0-13 (Sutherland, South Africa), 1m0-04, 1m0-05, 1m0-09 (Cerro Tololo, Chile); 1m0-03, 1m0-11 (Siding Spring, Australia)

Table A4. Photometric Data

Date	JD	mag	Filter	telescope	Date	JD	mag	Filter	telescope [a]
2013-06-03	2456446.788	14.116 0.002	V	1m0-4	2013-06-28	2456471.601	14.105 0.011	r	1m0-4
2013-06-04	2456447.788	14.123 0.018	V	1m0-4	2013-06-30	2456473.766	14.197 0.013	r	1m0-5
2013-06-05	2456448.789	14.152 0.008	V	1m0-4	2013-07-02	2456475.625	14.225 0.001	r	1m0-4
2013-06-06	2456449.788	14.169 0.001	V	1m0-4	2013-07-03	2456476.625	14.338 0.013	r	1m0-4
2013-06-07	2456450.793	14.160 0.019	V	1m0-4	2013-07-07	2456480.625	14.460 0.005	r	1m0-4
2013-06-09	2456452.789	14.375 0.014	V	1m0-4	2013-07-07	2456480.761	14.512 0.031	r	1m0-5
2013-06-12	2456455.789	14.333 0.003	V	1m0-4	2013-07-09	2456482.754	14.566 0.022	r	1m0-5
2013-06-16	2456459.660	14.427 0.009	V	1m0-9	2013-07-13	2456486.622	14.768 0.016	r	1m0-4
2013-06-20	2456463.661	14.449 0.010	V	1m0-4	2013-07-14	2456487.622	15.031 0.060	r	1m0-4
2013-06-22	2456465.595	14.550 0.011	V	1m0-4	2013-07-15	2456488.622	14.986 0.011	r	1m0-4
2013-06-24	2456467.595	14.523 0.003	V	1m0-4	2013-07-31	2456504.695	16.317 0.011	r	1m0-9
2013-06-26	2456469.595	14.565 0.036	V	1m0-4	2013-08-02	2456506.628	16.272 0.057	r	1m0-5
2013-06-28	2456471.595	14.642 0.008	V	1m0-4	2013-08-09	2456513.605	16.359 0.007	r	1m0-9
2013-06-30	2456473.761	14.710 0.018	V	1m0-5	2013-08-09	2456513.668	16.409 0.011	r	1m0-4
2013-07-02	2456475.619	14.848 0.006	V	1m0-4	2013-08-10	2456515.498	16.488 0.013	r	1m0-4
2013-07-03	2456476.619	14.904 0.004	V	1m0-4	2013-08-14	2456519.486	16.548 0.012	r	1m0-9
2013-07-07	2456480.619	15.092 0.007	V	1m0-4	2013-08-16	2456520.601	16.561 0.034	r	1m0-5
2013-07-09	2456482.748	15.219 0.027	V	1m0-5	2013-08-25	2456529.554	16.552 0.008	r	1m0-9
2013-07-13	2456486.616	15.550 0.014	V	1m0-4	2013-08-28	2456532.530	16.631 0.001	r	1m0-5
2013-07-14	2456487.616	15.670 0.002	V	1m0-4	2013-08-30	2456534.559	16.702 0.011	r	1m0-4
2013-07-15	2456488.616	15.772 0.006	V	1m0-4	2013-09-21	2456556.521	16.910 0.008	r	1m0-4
2013-07-17	2456490.616	16.141 0.023	V	1m0-4	2013-04-24	2456406.830	13.765 0.009	r	CSP
2013-07-19	2456492.623	16.600 0.022	V	1m0-4	2013-04-25	2456407.850	13.563 0.008	r	CSP
2013-07-29	2456502.616	17.311 0.020	V	1m0-4	2013-04-27	2456409.850	13.321 0.005	r	CSP
2013-07-29	2456502.624	17.336 0.022	V	1m0-9	2013-04-29	2456411.920	13.202 0.005	r	CSP
2013-08-02	2456506.620	17.345 0.046	V	1m0-5	2013-05-01	2456413.900	13.179 0.007	r	CSP
2013-08-09	2456513.594	17.337 0.020	V	1m0-9	2013-05-03	2456415.900	13.174 0.005	r	CSP
2013-08-09	2456513.658	17.466 0.018	V	1m0-4	2013-05-06	2456418.910	13.225 0.006	r	CSP
2013-08-10	2456515.487	17.610 0.030	V	1m0-4	2013-05-11	2456423.850	13.370 0.005	r	CSP
2013-08-14	2456519.474	17.587 0.020	V	1m0-9	2013-05-14	2456426.770	13.427 0.005	r	CSP
2013-08-16	2456520.589	17.560 0.003	V	1m0-5	2013-05-21	2456433.850	13.565 0.005	r	CSP
2013-08-25	2456529.543	17.550 0.012	V	1m0-9	2013-05-23	2456435.760	13.598 0.005	r	CSP
2013-08-28	2456532.518	17.723 0.011	V	1m0-5	2013-05-24	2456436.860	13.613 0.005	r	CSP
2013-08-30	2456534.548	17.659 0.072	V	1m0-4	2013-05-25	2456437.860	13.629 0.005	r	CSP
2013-09-21	2456556.509	17.922 0.057	V	1m0-4	2013-05-26	2456438.850	13.655 0.005	r	CSP
2013-09-24	2456559.569	18.071 0.017	V	1m0-4	2013-06-01	2456444.668	13.738 0.005	r	CSP
2013-04-25	2456407.578	13.486 0.010	r	1m0-10	2013-06-03	2456446.689	13.758 0.008	r	CSP
2013-04-25	2456408.464	13.391 0.004	r	1m0-10	2013-06-05	2456448.737	13.774 0.008	r	CSP
2013-04-26	2456409.462	13.304 0.008	r	1m0-10	2013-04-25	2456407.550	13.617 0.019	i	1m0-10
2013-04-27	2456410.463	13.314 0.014	r	1m0-10	2013-04-25	2456408.465	13.429 0.002	i	1m0-10
2013-04-29	2456412.499	13.159 0.017	r	1m0-10	2013-04-26	2456409.464	13.384 0.010	i	1m0-10
2013-05-03	2456415.785	13.120 0.007	r	1m0-4	2013-04-27	2456410.464	13.300 0.021	i	1m0-10
2013-05-03	2456415.864	13.177 0.002	r	1m0-5	2013-04-28	2456411.464	13.165 0.008	i	1m0-10
2013-05-04	2456416.823	13.167 0.034	r	1m0-5	2013-04-30	2456412.512	13.174 0.009	i	1m0-10
2013-05-05	2456417.786	13.121 0.011	r	1m0-4	2013-05-03	2456415.786	13.121 0.071	i	1m0-4
2013-05-06	2456418.785	13.180 0.026	r	1m0-4	2013-05-03	2456415.869	13.131 0.006	i	1m0-5
2013-05-11	2456423.749	13.355 0.004	r	1m0-9	2013-05-04	2456416.828	13.135 0.030	i	1m0-5
2013-05-15	2456427.748	13.482 0.005	r	1m0-9	2013-05-05	2456417.787	13.171 0.008	i	1m0-4
2013-05-31	2456443.720	13.678 0.009	r	1m0-9	2013-05-06	2456418.786	13.111 0.016	i	1m0-4
2013-06-03	2456446.793	13.739 0.009	r	1m0-4	2013-05-31	2456443.723	13.650 0.007	i	1m0-9
2013-06-04	2456447.793	13.726 0.001	r	1m0-4	2013-06-03	2456446.795	13.700 0.008	i	1m0-4
2013-06-05	2456448.793	13.792 0.009	r	1m0-4	2013-06-04	2456447.795	13.758 0.019	i	1m0-4
2013-06-07	2456450.798	13.764 0.012	r	1m0-4	2013-06-05	2456448.796	13.683 0.023	i	1m0-4
2013-06-09	2456452.795	13.777 0.012	r	1m0-4	2013-06-09	2456452.797	13.851 0.013	i	1m0-4
2013-06-12	2456455.795	13.849 0.002	r	1m0-4	2013-06-12	2456455.797	13.818 0.010	i	1m0-4
2013-06-16	2456459.671	13.913 0.010	r	1m0-9	2013-06-22	2456465.603	13.951 0.013	i	1m0-4
2013-06-20	2456463.671	14.005 0.006	r	1m0-4	2013-06-24	2456467.603	14.005 0.005	i	1m0-4
2013-06-22	2456465.601	14.021 0.018	r	1m0-4	2013-06-26	2456469.603	14.050 0.002	i	1m0-4
2013-06-24	2456467.601	14.076 0.016	r	1m0-4	2013-06-28	2456471.603	14.073 0.005	i	1m0-4
2013-06-26	2456469.601	14.063 0.010	r	1m0-4	2013-06-30	2456473.768	14.152 0.017	i	1m0-5

[a] *Swift* Telescope; CSP (Las Campanas, Chile); 1m0-08 (McDonald observatory, USA); 1m0-10, 1m0-12, 1m0-13 (Sutherland, South Africa), 1m0-04, 1m0-05, 1m0-09 (Cerro Tololo, Chile); 1m0-03, 1m0-11 (Siding Spring, Australia)

Table A5. Photometric Data

Date	JD	mag	Filter	telescope	Date	JD	mag	Filter	telescope [a]
2013-07-02	2456475.628	14.220 0.021	i	1m0-4	2013-04-24	2456406.830	13.916 0.013	i	CSP
2013-07-03	2456476.628	14.290 0.008	i	1m0-4	2013-04-25	2456407.850	13.663 0.008	i	CSP
2013-07-07	2456480.627	14.413 0.003	i	1m0-4	2013-04-27	2456409.840	13.371 0.006	i	CSP
2013-07-09	2456482.756	14.538 0.007	i	1m0-5	2013-04-29	2456411.920	13.216 0.005	i	CSP
2013-07-13	2456486.624	14.809 0.013	i	1m0-4	2013-05-01	2456413.900	13.145 0.005	i	CSP
2013-07-14	2456487.624	14.900 0.008	i	1m0-4	2013-05-03	2456415.900	13.127 0.005	i	CSP
2013-07-15	2456488.624	15.091 0.009	i	1m0-4	2013-05-06	2456418.910	13.181 0.006	i	CSP
2013-08-02	2456506.631	16.376 0.006	i	1m0-5	2013-05-11	2456423.850	13.351 0.006	i	CSP
2013-08-09	2456513.608	16.580 0.014	i	1m0-9	2013-05-14	2456426.770	13.420 0.005	i	CSP
2013-08-09	2456513.674	16.544 0.029	i	1m0-4	2013-05-21	2456433.850	13.570 0.005	i	CSP
2013-08-11	2456515.503	16.601 0.041	i	1m0-4	2013-05-23	2456435.770	13.599 0.005	i	CSP
2013-08-14	2456519.491	16.711 0.006	i	1m0-9	2013-05-24	2456436.860	13.610 0.006	i	CSP
2013-08-16	2456520.605	16.677 0.020	i	1m0-5	2013-05-25	2456437.860	13.632 0.005	i	CSP
2013-08-25	2456529.558	16.723 0.004	i	1m0-9	2013-05-26	2456438.860	13.657 0.005	i	CSP
2013-08-28	2456532.534	16.835 0.007	i	1m0-5	2013-06-01	2456444.669	13.754 0.005	i	CSP
2013-08-30	2456534.564	16.927 0.001	i	1m0-4	2013-06-03	2456446.691	13.754 0.008	i	CSP
2013-09-21	2456556.525	17.170 0.011	i	1m0-4	2013-06-05	2456448.739	13.787 0.006	i	CSP

[a] *Swift* Telescope; CSP (Las Campanas, Chile); 1m0-08 (McDonald observatory, USA); 1m0-10, 1m0-12, 1m0-13 (Sutherland, South Africa), 1m0-04, 1m0-05, 1m0-09 (Cerro Tololo, Chile); 1m0-03, 1m0-11 (Siding Spring, Australia)